Bioactive Materials 31 (2024) 578–589

Contents lists available at ScienceDirect

Bioactive Materials

journal homepage: www.keaipublishing.com/en/journals/bioactive-materials

Nanomotor-based H_2S donor with mitochondrial targeting function for treatment of Parkinson's disease

Zinan Zhao [1], Lin Chen [1], Chunhao Yang [1], Wenyan Guo, Yali Huang, Wenjing Wang, Mimi Wan [*], Chun Mao [**], Jian Shen [***]

National and Local Joint Engineering Research Center of Biomedical Functional Materials, School of Chemistry and Materials Science, Nanjing Normal University, Nanjing, 210023, China

ARTICLE INFO

Keywords:
Hydrogen sulfide donor
Mitochondrial targeting
Parkinson's disease
Blood brain barrier

ABSTRACT

Reduction of endogenous hydrogen sulfide (H_2S) is considered to have an important impact on the progress of Parkinson's disease (PD), thus exogenous H_2S supplementation is expected to become one of the key means to treat PD. However, at present, it is difficult for H_2S donors to effectively penetrate the blood brain barrier (BBB), selectively release H_2S in brain, and effectively target the mitochondria of neuron cells. Herein, we report a kind of nanomotor-based H_2S donor, which is obtained by free radical polymerization reaction between L-cysteine derivative modified-polyethylene glycol (PEG-Cys) and 2-methacryloyloxyethyl phosphorylcholine (MPC). This kind of H_2S donor can not only effectively break through BBB, but also be specifically catalyzed by cystathionine β-synthase (CBS) in neurons of PD site in brain and 3-mercaptopyruvate sulfurtransferase (3-MST) in mitochondria to produce H_2S, endowing it with chemotaxis/motion ability. Moreover, the unique chemotaxis effect of nanomotor can realize the purpose of precisely targeting brain and the mitochondria of damaged neuron cytopathic diseases. This kind of nanomotor-based H_2S donor is expected to enrich the current types of H_2S donors and provide new ideas for the treatment of PD.

1. Introduction

As an important signal molecule *in vivo*, endogenous hydrogen sulfide (H_2S) plays an important role in the progression of Parkinson's disease (PD). The reduction of endogenous H_2S level may lead to the reduction of sulfhydration modification and enzyme activity of Parkin protein, which involved in ubiquitination of proteins and is important for the survival of dopamine neurons, thus losing the ability to recognize toxic proteins and mediating the formation of α-synuclein (α-syn) aggregates. The formed α-syn aggregates will further aggregate in mitochondria, resulting in excessive reactive oxygen species (ROS) and neuroinflammation, thus damaging neurons [1–3]. Therefore, it is necessary to selectively supplement H_2S gas to damaged cells and their mitochondria for the treatment of PD.

Exogenous H_2S supplement can not only activate the proteasome pathway to degrade α-syn aggregates [3,4], but also mediate autophagy of damaged mitochondria in neurons, significantly reduce ROS level, eliminate neuroinflammation, and facilitate the repair of neurons [5–7]. With this regards, researchers have developed a variety of exogenous H_2S donors and tried to apply them to the treatment of neurodegenerative diseases [8–10]. As shown in Table S1, the earlier reported H_2S donors are mainly NaSH/Na_2S and GYY4137 that can release H_2S in aqueous solution, which are also the most commonly used H_2S donors in the treatment of neurodegenerative diseases [11]. However, such kinds of H_2S donors release H_2S in a short time (seconds to minutes), and cannot selectively release H_2S in brain, let alone effectively target mitochondria after reaching cells in brain [12]. Therefore, in order to reduce the consumption of donors in the process of blood circulation,

Peer review under responsibility of KeAi Communications Co., Ltd.
* Corresponding author.
** Corresponding author.
*** Corresponding author.
E-mail addresses: 2440741685@qq.com (Z. Zhao), 2437724798@qq.com (L. Chen), 1178094340@qq.com (C. Yang), 895979164@qq.com (W. Guo), 1322946555@qq.com (Y. Huang), wenjingwangg@163.com (W. Wang), wanmimi@njnu.edu.cn (M. Wan), maochun@njnu.edu.cn (C. Mao), jshen@njnu.edu.cn (J. Shen).
[1] These authors contributed equally: Zinan Zhao, Lin Chen, Chunhao Yang.

https://doi.org/10.1016/j.bioactmat.2023.09.001
Received 28 March 2023; Received in revised form 18 August 2023; Accepted 4 September 2023

many researchers chose to intracerebral injection during treatment process, which is invasive and difficult to be popularized to clinical applications [13,14]. In addition, researchers have also developed H_2S donors activated by free mercaptan, enzyme, ROS, pH, light and other methods [15], which may control the release of H_2S to a certain extent, but still cannot selectively release of exogenous H_2S in specific parts of the brain. Thus, most of the researches concerning these kinds of H_2S donors are at the *in vitro* level, and are rarely used for the treatment of brain diseases [16–18]. Although exogenous H_2S supplementation is expected to treat PD from multiple perspectives by interfering with the neuron cell protease system, it is still a great challenge to design H_2S donors that can be administered intravenously, effectively pass through the blood brain barrier (BBB), selectively release of exogenous H_2S in the brain section, and effectively target the mitochondria of neuron cells due to the shortage of H_2S donors.

Based on this, we designed a kind of nanomotor-based H_2S donor, which was mainly obtained by free radical polymerization reaction between polyethylene glycol (PEG) modified with L-cysteine derivative (PEG-Cys) and 2-methacryloyloxyethyl phosphorylcholine (MPC) (denoted as PCM). Among them, the presence of PEG could prolong the blood circulation time of the nanomotor-based H_2S donor [19]. Further, thanks to the particularity of MPC, which was similar to acetylcholine and choline in structure, it could make use of the interaction between acetylcholine or choline and nAChRs (nicotinic acetylcholine receptors) or ChTs (choline transporters) on the surface of cerebral vascular endothelial cells to achieve of the goal of penetrating BBB for H_2S donor (Fig. 1a) [20–22]. After entering the neuron cells, the specific affinity between 3-mercaptopyruvate sulfurtransferase (3-MST, specifically expressed in mitochondria) and L-cysteine could be used for further targeting of the nanomotor-based H_2S donor, this is because 3-MST has higher catalytic capacity ability to produce H_2S than CBS [23]. Therefore, the nanomotor-based H_2S donor could achieve effective targeting of mitochondria, more accurately deliver H_2S to the diseased mitochondria of damaged neuron cells, to better play a therapeutic role (Fig. 1b). In particular, the content of CBS in serum and vascular endothelial cells was far lower than that in neuron cells, thus achieved a certain degree of selective release of H_2S in the brain and reduced unnecessary release of H_2S during blood circulation [24].

2. Results and discussion

2.1. Characterizations of the nanomotor-based H_2S donor

First, L-cysteine and methacryloyl chloride were condensed to obtain 2-methacryloyl amino cysteine (M-Cys), its structure was confirmed by ^1H NMR spectrum (Fig. S1a), ^{13}C NMR spectrum (Fig. S2) and Fourier transform infrared (FTIR) spectroscopy (Fig. S1b). Specifically, C═O stringing vibration (amide-I band) was observed at 1736 cm^{-1}, –SH stringing and N–H (secondary amine group) stringing vibration were observed at 2550 cm^{-1} and 3421 cm^{-1} [25,26]. In order to prolong the blood circulation time of the final product, M-Cys was connected to PEG-NH_2 to obtain PEG-Cys monomer. PEG-Cys and MPC were cross-linked by free radical polymerization under the action of cross-linking agent N, N′-bis (acryloyl) cystamine (BAC) to form poly (PEG-Cys-MPC) (PCM), namely nanomotor-based H_2S donor. The structure of PEG-Cys and nanomotor-based H_2S donor PCM were characterized by FTIR spectroscopy (Fig. S3). Specifically, C–O–C stretching vibration and C═O stretching vibration (amide-I band) in PEG-Cys structure were observed at 1112 cm^{-1} and 1720 cm^{-1}, The main absorption peaks of nanomotor-based H_2S donor PCM included the –SH characteristic absorption peak (2651 cm^{-1}) of L-Cysteine, C–O–C stretching vibration (1225 cm^{-1}) of PEG, the typical amido-I band

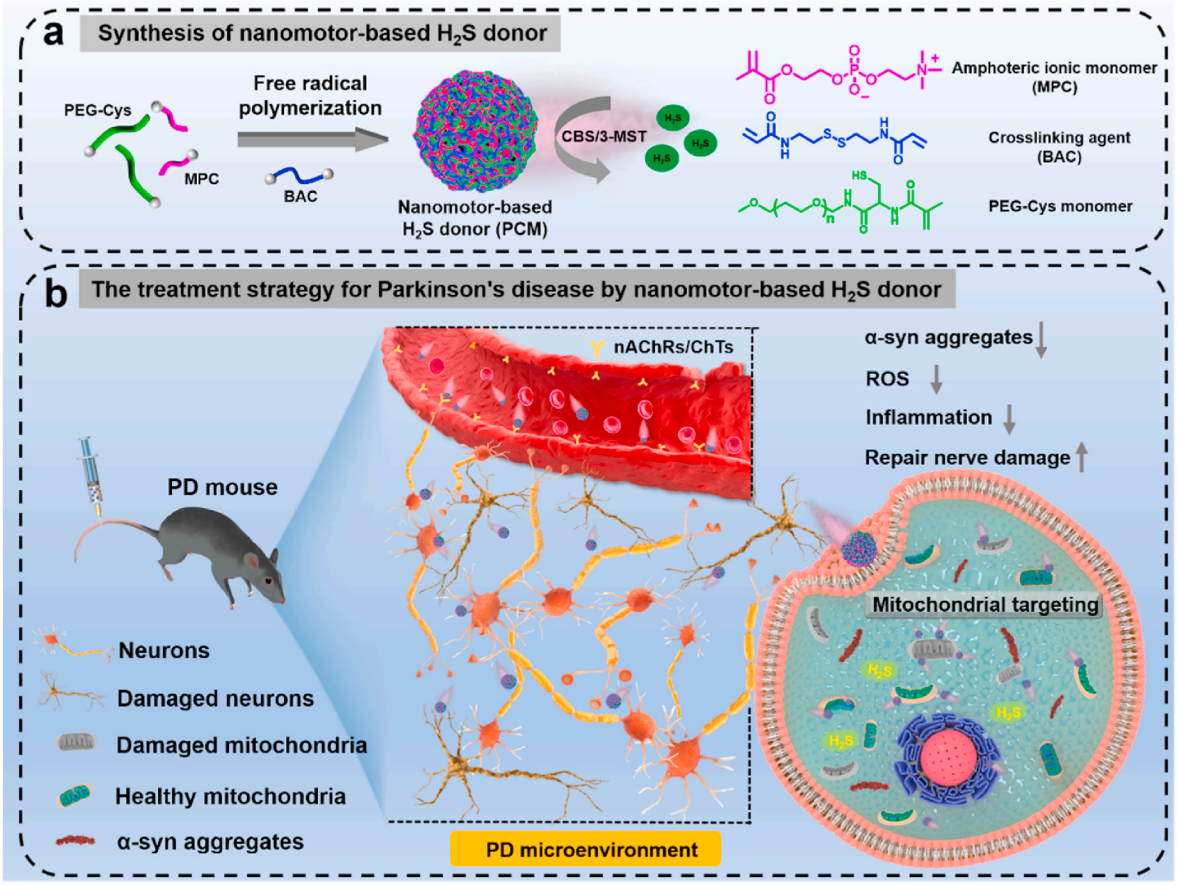

Fig. 1. Illustration of the synthetic process of nanomotor-based H_2S donor PCM and the treatment strategy for PD.

(1650 cm^{-1}) of BAC and the bending vibration of -$POCH_2$- bond at 1085 cm^{-1} in MPC structure [27–29]. TEM image showed that nanomotor-based H_2S donor PCM was a spherical particle with a diameter of about 100 nm (Fig. 2a). For comparison, we also synthesized poly (PEG-Thr-MPC) (PTM) nanoparticles that didn't have the ability to produce H_2S and motion. Instead of L-Cysteine, we used L-Threonine that had a similar structure with L-Cysteine but didn't have –SH group. The structures of N-Methacryloyl-L-Threonine (M-Thr) and PEG-Thr could be confirmed by ^1H NMR spectrum (Fig. S4a) and FTIR spectroscopy (Fig. S4b), in which 1640 cm^{-1} and 1112 cm^{-1} corresponded to C═O stretching vibration (amide-I band) and C–O–C stretching vibration in the PEG-Thr structure [28,29]. The size (about 100 nm) and surface charge (about −9.36 mV) of non-nanomotor PTM were similar to those of nanomotor-based H_2S donor PCM (Fig. 2b and c). Subsequently, the ability of the nanomotor-based H_2S donor PCM to release H_2S in the cell environment was tested. In the BV2 cell and stimulated SH-SY5Y cell environment, H_2S could be released for 24 h, and the release amount could reach 6.16 μM and 7.65 μM (Figs. S6 and 2d), which was much higher than that of H_2S donors triggered by free mercaptan and enzyme (usually less than 4 h) [30–33]. In particular, the selective release of H_2S from different cells by nanomotor based H_2S donor PCM was examined. As shown in Fig. 2e, the amount of H_2S released by nanomotor-based H_2S donor in neuron cells was much higher than that in HUVECs, bEnd.3 cells, respectively. These results may be owing to the fact that CBS and 3-MST were the main enzymes to produce endogenous H_2S in brain environment, and the expression of these two enzymes in brain endothelial cells was less [24].

Since the presence of zwitterions in nanomotor-based H_2S donor PCM substrate could provide it with anti-protein adhesion property [34,35], we used particle size analysis and CLSM to detect this property. As shown in Fig. 2f, nanomotor-based H_2S donor PCM (hydrated particle size was about 200 nm) and BSA (about 6.5 nm and 1.4 μm) were co-incubated, the particle size distribution results showed three independent peaks, indicating that the nanomotor-based H_2S donor PCM didn't adsorb proteins and maintained its original size. The CLSM image in Fig. 2g additionally showed this result. The red fluorescence representing the nanomotor-based H_2S donor PCM, the green fluorescence representing BSA were independent of each other, and there was no obvious overlap, which confirmed that the nanomotor-based H_2S donor PCM had good anti-albumin adhesion performance, which may enable PCM to have anti-protein adhesion ability in the process of blood circulation.

Furthermore, the movement behavior of nanomotor-based H_2S donor PCM in different cells was explored. We evaluated the movement of nanomotor-based H_2S donor PCM in PBS, bEnd.3 cells and neuron cells (SH-SY5Y cells) environment, as well as the movement ability of non-nanomotor PTM in SH-SY5Y cell environment. The results showed that nanomotor-based H_2S donor PCM had typical Brownian motion

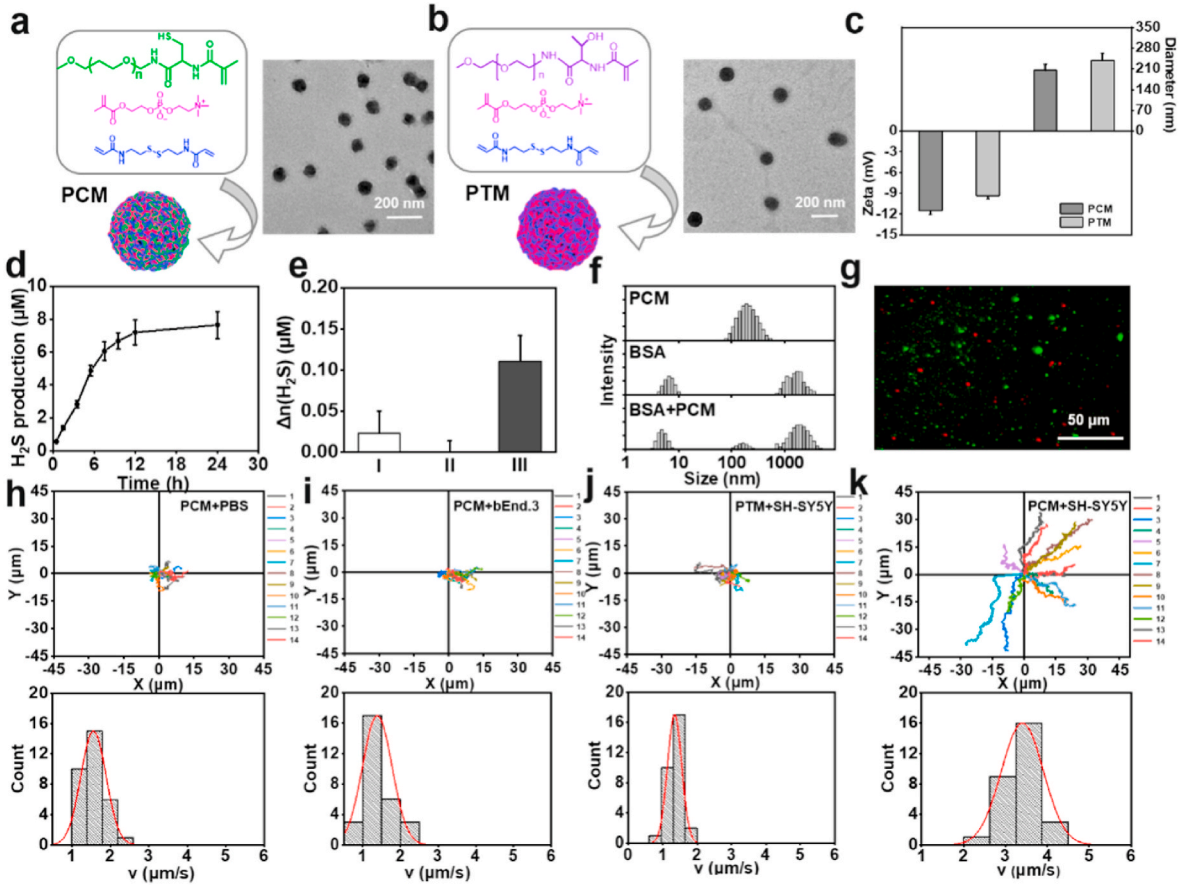

Fig. 2. Characterizations of different samples. TEM images of a) nanomotor-based H_2S donor PCM, b) non-nanomotor PTM; c) Zeta and DLS results of different samples; d) Accumulative H_2S release curve of nanomotor-based H_2S donor PCM incubated in stimulated SH-SY5Y cells environment for different times; e) The net production of H_2S with the addition of nanomotor-based H_2S donor PCM in different kinds of cells for 24 h ($\Delta c_{(H2S)}$ (μM) = $c_{(\text{cells co-incubated with PCM})} - c_{(\text{blank cells})}$), I: HUVECs; II: bEnd.3; III: SH-SY5Y); f) DLS results of nanomotor-based H_2S donor PCM (1 mg mL^{-1}) and BSA (500 mg mL^{-1}) incubated at 37 °C for 4 h and g) CLSM image of the mixture of Cy5-maleimide labeled nanomotor-based H_2S donor PCM (1 mg mL^{-1}, red) and FITC labeled BSA (500 mg mL^{-1}, green) incubated at 37 °C for 4 h (the solution was diluted for 1000 times to capture image); Motion trace diagram (top, n = 14) of nanomotor-based H_2S donor PCM in h) PBS, i) bEnd.3 cells and velocity distribution diagram (bottom, n = 30) under this condition; Motion trace diagram (top, n = 14) of j) non-nanomotor PTM, and k) nanomotor-based H_2S donor PCM in stimulated SH-SY5Y cells environment and velocity distribution diagram (bottom, n = 30) under this condition.

behavior in the PBS and bEnd.3 cells environment (Fig. 2h and i, Video S1, Video S2), and non-nanomotor PTM without movement ability also showed similar Brownian motion behavior in SH-SY5Y cells (Fig. 2j, Video S3). In contrast, nanomotor-based H_2S donor PCM showed obvious motion tracks in SH-SY5Y cells (Fig. 2k, Video S4). We also selected 30 particles to calculate their speed distribution. It could be seen from the speed distribution in Fig. 2j and k that non-nanomotor PTM velocity distribution was concentrated in 1.5 μm s^{-1}, while nanomotor-based H_2S donor PCM velocity distribution was concentrated in 3.5 μm s^{-1}.

2.2. Cellular uptake of nanomotor-based H_2S donor and its ability to penetrate the BBB in vitro

After determining the selective release of H_2S and movement ability of nanomotor-based H_2S donor PCM in neurons, we continued to evaluate its ability to pass through the BBB *in vitro*. Firstly, we studied that the movement ability of the nanomotor-based H_2S donor PCM can promote the uptake behavior of cells. As shown in Fig. 3a and S8, the uptake of nanomotor-based H_2S donor PCM and non-nanomotor PTM by brain endothelial cells (bEnd.3 cells) didn't show a significant difference. The possible reason may be that the bEnd.3 cells didn't highly express CBS, and nanomotor-based H_2S donor PCM couldn't show typical motion behavior, therefore, the uptake of cells was similar to that of non-nanomotors PTM (Fig. 3b). For neurons with high expression of CBS (SH-SY5Y cells), the intracellular fluorescence intensity after co-incubation with nanomotor-based H_2S donor PCM was 7.6 times higher than that of co-incubation with non-nanomotor PTM (Fig. 3c, d, S9), indicating that the movement effect of nanomotor could make it more easily enter neurons selectively. Subsequently, we continued to evaluate the ability of different samples to penetrate the BBB model *in vitro*. bEnd.3 cells were inoculated on the upper layer of the Transwell chamber and incubated for 10 days to form an *in vitro* model simulating BBB. Then, the stimulated SH-SY5Y cells were inoculated on the lower layer (Fig. 3e) [36–38]. After adding different samples labeled with Cy5-maleimide to the upper layer for 24 h, CLSM was used to observe the red fluorescence signal of Cy5-maleimide in the stimulated SH-SY5Y cells on the lower layer. As shown in Fig. 3f–g, both nanomotor-based H_2S donor PCM and non-nanomotor PTM could penetrate bEnd.3 cells to reach SH-SY5Y cells in the lower chamber, but the former showed more obvious red fluorescence intensity, indicating that nanomotor-based H_2S donor PCM was more easily absorbed by SH-SY5Y cells after penetration.

Further, different endocytosis inhibitors were used to treat SH-SY5Y cells to explore the main pathways through which this type of H_2S donor enters the neuron cells. After the cells were co-incubated with nanomotor-based H_2S donor PCM, we inferred the main pathway for this type of H_2S donor to enter the cells by detecting the changes in the uptake efficiency of the cells to nanomotor-based H_2S donor PCM. The involved endocytosis inhibitors include chlorpromazine (clathrin endocytosis inhibitor, Chlor.), nystatin (caveolin endocytosis inhibitor), cytochrome D (macropinocytosis inhibitor, Cyto. D), mecamylamine (acetylcholine receptor antagonist) and 4 °C low temperature (energy inhibition) [39,40]. As shown in Fig. 3h, i and S10, chlorpromazine, mecamylamine and 4 °C low temperature treatment significantly inhibited the uptake of nanomotor-based H_2S donor PCM by SH-SY5Y cells, while the uptake of nanomotor-based H_2S donor PCM by adding nystatin and cyto. D changed little. This result suggested that the main pathway for the nanomotor-based H_2S donor PCM to enter SH-SY5Y cells depended on the endocytosis mediated by clathrin protein and acetylcholine receptor. Low temperature treatment at 4 °C reduced the uptake of nanomotor-based H_2S donor PCM by SH-SY5Y cells, which might be due to the reduction of cell metabolism and membrane fluidity under low temperature conditions, leading to the inhibition of energy-dependent endocytosis [41].

2.3. Mitochondrial targeting behavior of nanomotor-based H_2S donor in cellular models

Mitochondrial dysfunction is an essential cause of PD. It is very important for therapeutics to escape from lysosome phagocytosis and target mitochondria after entering cells. Therefore, the location of nanomotor-based H_2S donor PCM after entering the SH-SY5Y cells was characterized. As shown in Fig. 4a and S11, after the non-nanomotor PTM entered the SH-SY5Y cells, the red fluorescence representing the non-nanomotor PTM was highly coincident with the green fluorescence representing the lysosome, while there were only a few red signals at the Golgi and mitochondria positions, which indicated that the non-nanomotor PTM without movement ability would stay in the lysosome to a large extent after entering the cell. In contrast, after nanomotor-based H_2S donor PCM with movement ability entered the SH-SY5Y cells, only a small amount of red fluorescence was coincident with the green fluorescence of lysosome, some would stay in Golgi, and more red fluorescence signals were coincident with the green mitochondrial fluorescence. This result showed that the movement ability of nanomotors could promote them to escape lysosome phagocytosis and effectively gather in mitochondria. The co-localization of nanomotor-based H_2S donor PCM and Golgi was conducive to their transfer between cells.

Furthermore, we used the "Y" channel to characterize the chemotactic targeting ability of nanomotor-based H_2S donor PCM to mitochondria [42,43]. As shown in Fig. 4b, the three chambers of channel "Y" were set as follows: chamber I is nanomotor-based H_2S donor PCM or non-nanomotor PTM, chamber II is the lysate extracted from mitochondria, and chamber III is the lysate of all substances except mitochondria. When non-nanomotor PTM without movement ability and mitochondrial targeting ability was placed in chamber I, chamber II and chamber III showed similar weak fluorescence intensity (Fig. 4c and d). When the chamber I was placed with nanomotor-based H_2S donor PCM with mitochondrial targeting capability, it could target chamber II (mitochondrial lysate) extremely clearly within 60 min (Fig. 4c and e), suggesting that nanomotor-based H_2S donor PCM had strong targeting capability.

2.4. Promotion effect on neuronal cell growth and differentiation by nanomotor-based H_2S donor in cellular models

We confirmed that nanomotor-based H_2S donor PCM with movement ability could be better captured by neuron cells, so we continued to explore whether the nanomotor-based H_2S donor PCM can promote the repair of damaged neuron cells. In order to better demonstrate the ability of movement behavior to promote the role of H_2S, we selected the small molecule H_2S donor GYY4137 commonly used *in vivo* as a comparison [44]. At the same time, GYY4137 was loaded on the non-nanomotor PTM as a control sample of H_2S donor without movement ability (under the same conditions, the amount of H_2S released was equivalent, so it was named non-nanomotor based H_2S donor (PTM@G)). First, the ability of nanomotor-based H_2S donor PCM to eliminate ROS after entering the cells was evaluated. As shown in Fig. 5a and S12, the nanomotor-based H_2S donor PCM with movement ability could effectively reduce the production of ROS in stimulated SH-SY5Y cells. Compared with other groups, the green fluorescence that represented intensity of ROS was significantly reduced in the nanomotor-based H_2S donor PCM treatment group, and its treatment effect was much better than that of small molecule H_2S donor GYY4137 (Fig. 5b). Next, the effects of different concentrations of nanomotor-based H_2S donor PCM on cell viability of bEnd.3 cells and SH-SY5Y cells were studied. As shown in Fig. 5c, when the concentration of nanomotor-based H_2S donor PCM reached 0.8 mg mL^{-1}, the bEnd.3 cell viability was not significantly affected, which proved that nanomotor-based H_2S donor PCM had good cell compatibility. It is worth noting that with the concentration of nanomotor-based H_2S donor

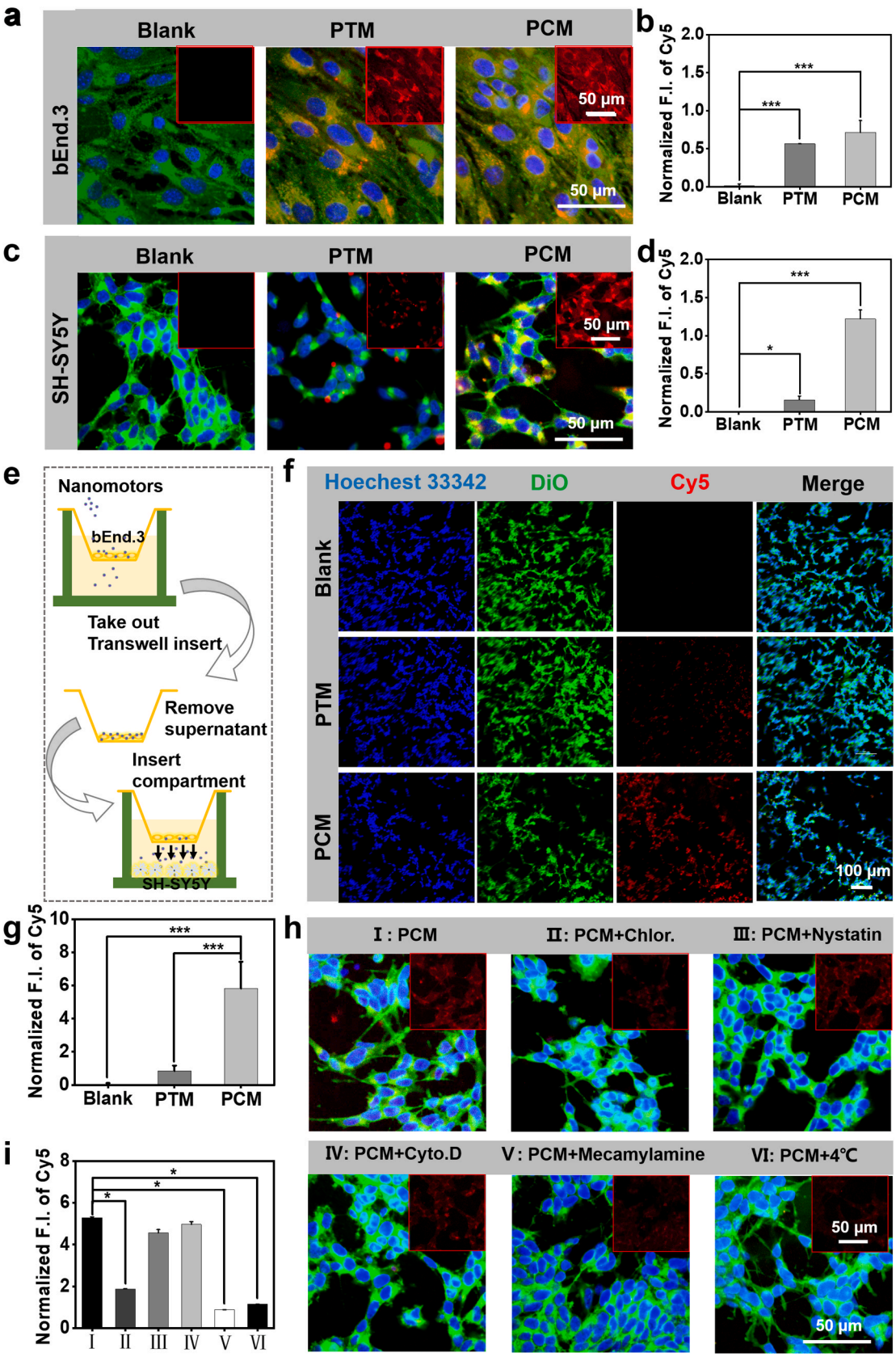

(caption on next page)

Fig. 3. Penetration behavior of BBB model *in vitro*. a) CLSM images (merged images) of different samples incubated with bEnd.3 cells for 24 h (the inserted images represent the single channel of different samples); b) Analysis of red fluorescence intensity of different samples in bEnd.3 cells (n = 3); c) CLSM images (merged images) of different samples incubated with stimulated SH-SY5Y cells for 24 h; d) Analysis of red fluorescence intensity of different samples in SH-SY5Y cells (n = 3), and the blank group represents the group without added samples (Blue: Hoechst 33342-nucleus; Green: DiO-cell membrane; Red: samples. The inserted image: single channel of image for samples); e) Schematic illustration of Transwell model simulating BBB *in vitro*; f) CLSM images of SH-SY5Y cells in the lower layer of Transwell model and g) red fluorescence intensity analysis of different samples (n = 3). h) CLSM images (merged images) of SH-SY5Y in the presence of different inhibitors (Blue: Hoechst 33342-nucleus; Green: DiO-cell membrane; Red: Nanomotor-based H_2S donor PCM, the inserted images represent the single channel of different samples) and i) red fluorescence intensity analysis of nanomotor-based H_2S donor PCM (I: Nanomotor-based H_2S donor PCM; II: Nanomotor-based H_2S donor PCM + Chlor.; III: Nanomotor-based H_2S donor PCM + Nystatin; IV: Nanomotor-based H_2S donor PCM + Cyto.D; V: Nanomotor-based H_2S donor PCM + Mecamylamine; VI: Nanomotor-based H_2S donor PCM+4 °C) (n = 3). *$p < 0.05$, **$p < 0.01$, and ***$p < 0.001$.

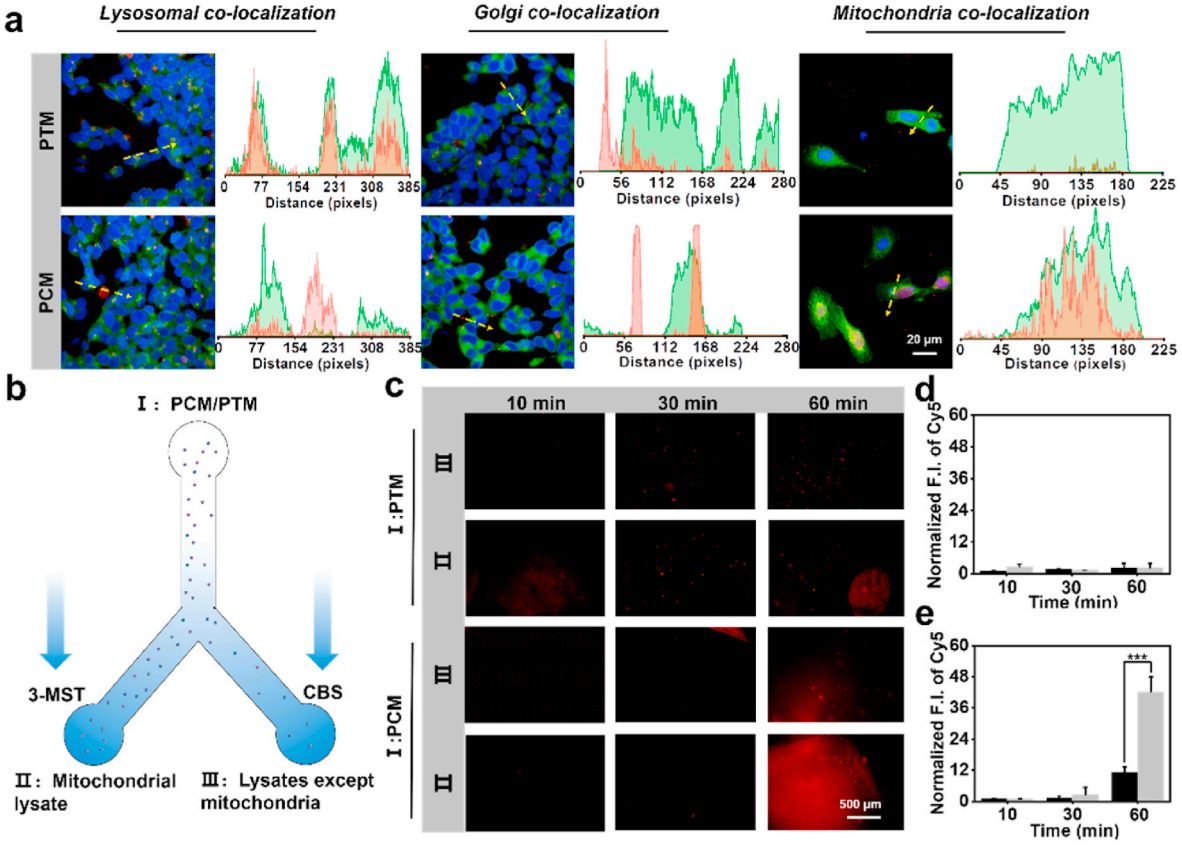

Fig. 4. Characterization of organelle co-localization and mitochondria targeting ability of nanomotor-based H_2S donor PCM. a) CLSM images of co-localization of nanomotor-based H_2S donor PCM with major organelles (lysosomal, Golgi, mitochondria) and corresponding fluorescence curves for the section marked with yellow line (Blue: Hoechst 33342-nucleus; Green: lysosomal/Golgi/mitochondria; Red: samples); b) Schematic illustration for "Y" channel (I: nanomotor-based H_2S donor PCM/non-nanomotor PTM; II: Mitochondrial lysate; III: Lysates except mitochondria); c) Fluorescent images of different samples at the end of "Y" channel within 60 min; Fluorescence intensity quantification of d) non-nanomotor PTM and e) nanomotor-based H_2S donor PCM at the end of "Y" channel at different time points (n = 3). *$p < 0.05$, **$p < 0.01$, and ***$p < 0.001$.

PCM increased to 0.4 mg mL^{-1} or above, the SH-SY5Y cell viability decreased slightly (Fig. 5d). This might be because the high concentration of nanomotor-based H_2S donor PCM can produce a higher concentration of H_2S, which has a negative impact on cell survival. Therefore, 0.2 mg mL^{-1} nanomotor-based H_2S donor PCM was selected as the therapeutic concentration. Subsequently, we continued to explore the effect of nanomotor-based H_2S donor PCM on the cell activity of stimulated SH-SY5Y cells after co-incubation at this concentration for different times. It could be seen from Fig. 5e that compared with the cell activity of the simple stimulation group, the SH-SY5Y cell activity significantly increased (from 47.8% to 79.2%) after co-incubation with nanomotor-based H_2S donor PCM for 12 h, which might be because nanomotor-based H_2S donor PCM reduced ROS production of cells in the stimulation group. It could be seen from Fig. 5f that after co-incubation of different samples with stimulated SH-SY5Y cells for 24 h, the cell viability of the nanomotor-based H_2S donor PCM group was significantly higher than that of other sample groups, which also verified that the nanomotor-based H_2S donor PCM as a new generation of H_2S donor had better therapeutic effect *in vitro*.

Next, we evaluated in detail the influence of nanomotor-based H_2S donor PCM on the growth and differentiation of neuron cells. SH-SY5Y cells were differentiated into nerve cells using 12-0-tetracanoyl-phorbol-13-acetate (TPA) to study the growth and differentiation of nerve cells [45,46]. As shown in Fig. 5g, after treatment with GYY4137, non-nanomotor-based H_2S donor PTM@G and nanomotor-based H_2S donor PCM, the length of neurites of SH-SY5Y cells were higher than that of the model group. Among them, the length of neurites in the nanomotor-based H_2S donor PCM group was 20.39 μm increased to 54.24 μm and equivalent to blank cells without stimulation. At the same time, we also observed the cell differentiation rate, the number of new neurites and the length of neurites in the differentiated cells of stimulated SH-SY5Y cells within 6 days. As shown in Fig. 5h–j, on the 6th day of treatment, the cell differentiation rate, the number of new neurites and the length of neurites in the nanomotor-based H_2S donor PCM group

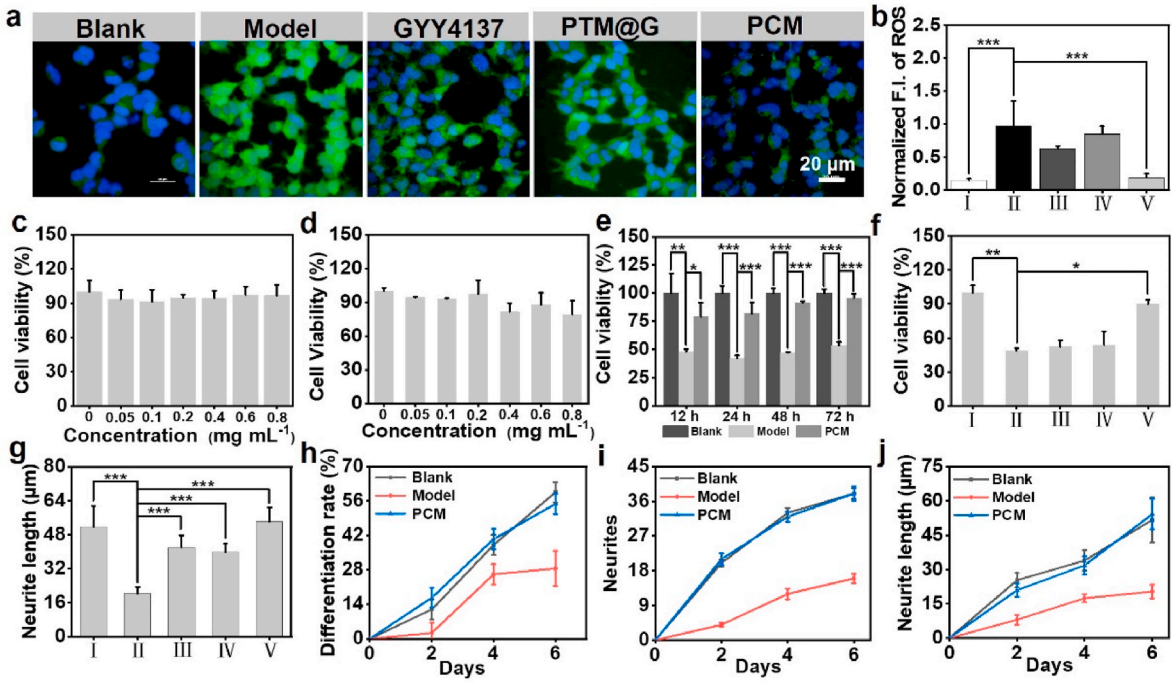

Fig. 5. Promotion effect on neuronal cell growth and differentiation by nanomotor-based H_2S donor in cellular models. a) CLSM images of intracellular ROS after 24 h co-incubation of different samples with stimulated SH-SY5Y cells (Blue: Hoechst 33342-nucleus; Green: DCFH-DA-ROS) and b) The corresponding fluorescence intensity of ROS in a) (n = 3); Effects of different concentrations of nanomotor-based H_2S donor PCM on cell viability of c) bEnd.3 cells and d) SH-SY5Y cells; e) Cell viability of stimulated SH-SY5Y cells after co-incubated with nanomotor-based H_2S donor PCM (0.2 mg mL^{-1}) for different times (n = 3); f) Cell viability of stimulated SH-SY5Y cells after co-incubated with different samples for 24 h; g) Neurite length of SH-SY5Y cells treated by different samples for 6 days. (n = 5); h) Differentiation rate, i) Neurites, and j) Neurite length of SH-SY5Y cells treated by nanomotor-based H_2S donor PCM over 6 days; The blank group represented SH-SY5Y cells without the stimulated treatment, model and the other groups represented SH-SY5Y cells with the stimulated treatment. I: Blank; II: Model; III: GYY4137; IV: Non-nanomotor-based H_2S donor PTM@G; V: Nanomotor-based H_2S donor PCM. $^*p < 0.05$, $^{**}p < 0.01$, and $^{***}p < 0.001$.

were similar as those of the blank group. The results confirmed that nanomotor-based H_2S donor PCM could participate in the repair process of nerve cells and promote their growth and differentiation.

2.5. Therapeutic effect of nanomotor-based H_2S donor in MPTP-induced PD model mice

We confirmed *in vitro* that nanomotor-based H_2S donor PCM had the ability to break through BBB, enter neurons more quickly and target mitochondria of neurons. We contiuned to evaluate the targeting and therapeutic performance of this type of H_2S donor in PD model *in vivo* (Fig. 6a). First, the ability of nanomotor-based H_2S donor PCM to target the brain of PD mice was evaluated. Cy5-maleimide labeled nanomotor-based H_2S donor PCM and non-nanomotor PTM were injected into the body of PD mice through tail vein. After the brain and other important organs were ground, the fluorescence intensity of the grinding solution was measured with a fluorescence spectrophotometer to calculate the brain delivery efficiency and biodistribution of different samples. As shown in Fig. 6b, within 24 h after the tail vein injection of different samples, the accumulation of nanomotor-based H_2S donor PCM in the brain was significantly higher than that of non-nanomotor PTM. The brain delivery efficiency of nanomotor-based H_2S donor PCM was 21.3% ID (the percentage of injected dose), while that of non-nanomotor PTM was only 13.6% ID. Within 48 h after tail vein injection, the accumulation of nanomotor-based H_2S donor PCM in the brain could still maintain 18.1% ID. This might be because under the action of MPC, both nanomotor-based H_2S donor PCM and non-nanomotor PTM can pass through the BBB. However, the nanomotor-based H_2S donor PCM has the chemotaxis ability to CBS and 3-MST highly expressed in the brain, and the resulting movement ability enabled it to be more absorbed by nerve cells and stayed in the brain to play a role. In addition, the biodistribution of different samples showed that all samples were mainly accumulated in the liver and kidney, the metabolic organs of mice (Fig. 6c and d). Then, we tested the pharmacokinetic curve of nanomotor-based H_2S donor PCM (Fig. S13), and the results showed that this kind of nanomotor could be stable in the blood for at least 30 h. The western blotting results of Fig. S14 indicated that, compared to the aorta, the high expression of CBS in the midbrain enabled nanomotor-based H_2S donor PCM to release H_2S in the brain rather than in the blood circulation process.

Subsequently, we evaluated the treatment effect of nanomotor-based H_2S donor PCM on PD mice from the aspects of spontaneous movement, motion coordination and memory improvement, and selected the open field test, pole test and Morris water make test [27,47]. The treatment process of PD mice induced by MPTP was shown in Fig. 6a. After 10 days of continuous intraperitoneal injection of MPTP, different samples were injected by the tail vein for 7 days, and the evaluation began on the 18th day. We observed and recorded the movement track of mice in the open field to evaluate the spontaneous activity of mice. The normal group represent healthy mice, and the model group represent PD mice induced by MPTP. As shown in Fig. 6e, compared with normal mice, the pathway of PD mice showed the behavior of wall-to-wall behavior. The movement behavior of mice treated with different types of H_2S donors can be improved to a certain extent, which were shown the similar movement track to normal mice, but the movement track of mice treated with nanomotor-based H_2S donor PCM was the closest to that of normal mice. From the average speed and total distance of this process, it can be more intuitively seen that different types of H_2S donors have different therapeutic effects. The average speed (4.3 cm s^{-1}) and total distance (2.6 m) of the model group mice in the open field were significantly lower than those of normal group (9.8 cm s^{-1}, 5.9 m), which meant that the spontaneous motor activities of the model group mice induced by MPTP were significantly affected. The average speed (5.8 cm s^{-1}) and total distance (3.5 m) of mice treated with free small molecule H_2S donor

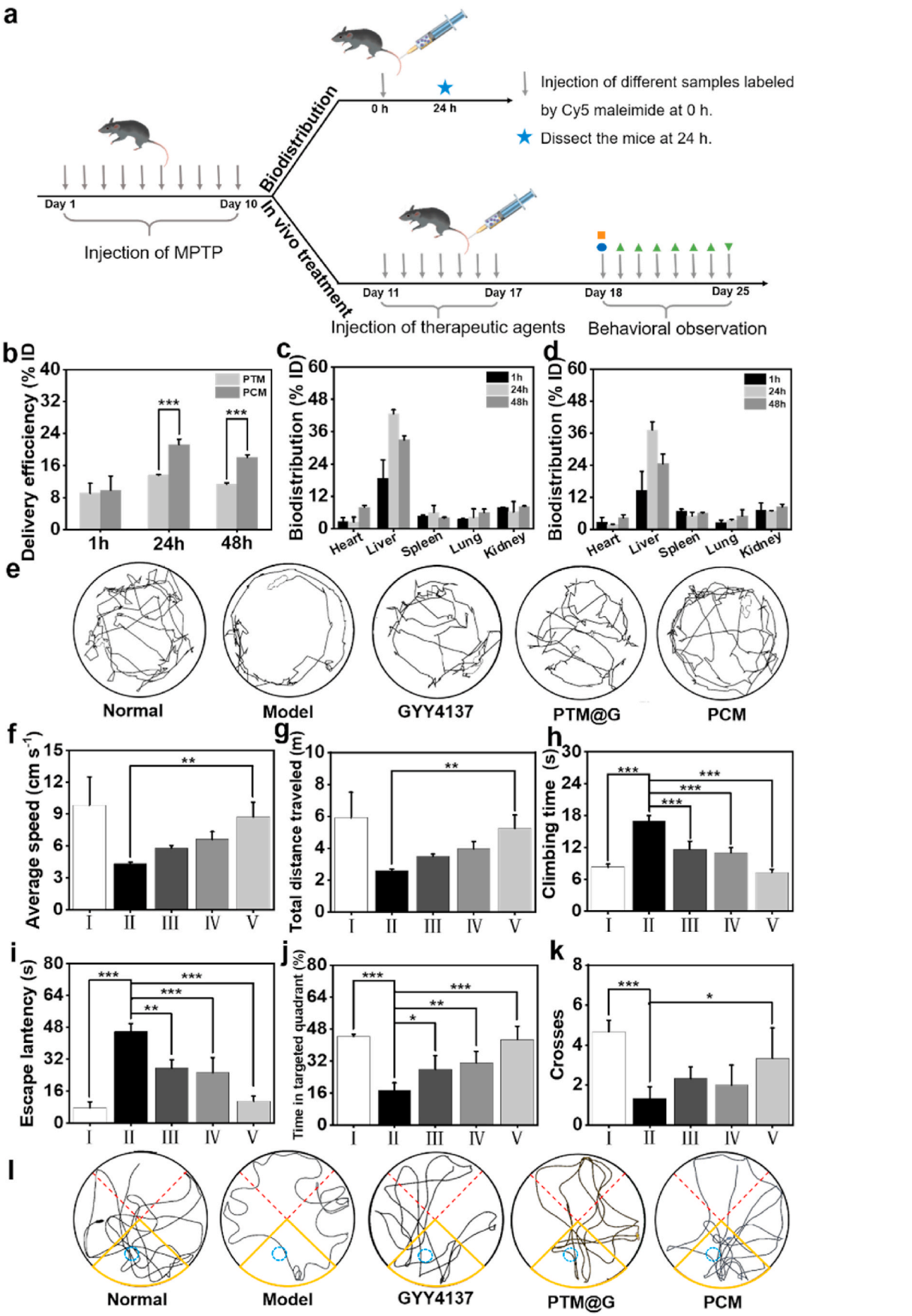

(caption on next page)

Fig. 6. *In vivo* targeting efficiency of different samples and behavioral improvement of MPTP-induced PD model mice. a) Schematic illustration of the *in vivo* targeting ability and therapeutic effect evaluation. Circular: the open field; Square: the pole test; Upward triangle: Morris water maze training; Inverted triangle: Morris water maze test; b) Brain delivery efficiency of different samples labeled with Cy5 maleimide after tail vein injection for different time (n = 3); Biodistribution of c) non-nanomotor PTM and d) nanomotor-based H_2S donor PCM labeled with Cy5 maleimide after tail vein injection for 24 h (n = 3); e) Representative open-field traveled trace, f) Average speed, and g) total distance traveled of mice by different treatment in open field instrument (n = 3); h) The climbing time it took the mice to climb to the top in pole test (n = 3); i) Escape latency (n = 3); j) Swimming time spent in the targeted quadrant, k) Crossed over the platform of mice by different treatment (n = 3) and l) Representative swimming path tracing of mice by different treatments (the blue circle: the platform site; the yellow line: the targeted quadrant; the black line: the trace tracking). I: Normal; II: Model; III: GYY4127; IV: Non-nanomotor PTM@G; V: Nanomotor-based H_2S donor PCM. All statistical data were presented as mean ± standard deviation. $^*p < 0.05$, $^{**}p < 0.01$, and $^{***}p < 0.001$.

GYY4137 were improved. Non-nanomotor-based H_2S donor PTM@G treatment effect could be further improved, with the average speed and total distance increased to 6.6 cm s^{-1} and 4.0 m respectively. The average speed and total distance of mice treated with nanomotor-based H_2S donor PCM could be increased to 8.7 cm s^{-1} and 5.2 m, showed the best therapeutic effect (Fig. 6f and g). In the pole test (Fig. 6h), which represented the motion coordination ability of mice, the average time for the model group mice to climb to the bottom of the pole was about 17 s, which was much longer than the time required by the normal mice (about 8 s), indicating that the motion coordination ability of the model group mice was impaired. After the treatment with three different forms of H_2S donors, the motion coordination ability could be improved. Among them, the average time (about 7 s) of mice in the nanomotor-based H_2S donor PCM group to climb to the bottom of the pole was equivalent to that of normal mice, indicating that the motion coordination ability of mice was significantly improved. In the Morris water maze test, which represents the memory function of mice, the memory improvement of mice was evaluated by the escape time, the time staying in the target quadrant and the frequency of mice crossing the original platform position during the platform free period. As shown in Fig. 6i–k, the spatial memory ability of mice after treatment with nanomotor-based H_2S donor PCM was significantly improved. Compared with the model group, the escape time of mice in the nanomotor-based H_2S donor PCM treatment group was significantly shortened (from 46 s to 11 s), the percentage of stay time in the target quadrant during the platform free period was longer (from 17% to 42%), and they crossed the original platform position for many times (from 1 time to 3 times), indicating that the memory function had been significantly improved. Moreover, compared with other treatment groups, the movement path of mice in the nanomotor-based H_2S donor PCM treatment group in the water maze was mainly focused on the target quadrant, which indicated that nanomotor-based H_2S donor PCM could induce the recovery of spatial memory impairment in PD mice (Fig. 6l).

In addition to using mice ethology to evaluate the H_2S released by nanomotor-based H_2S donor PCM could effectively play a therapeutic role in PD, we further tested several indicators of the mouse brain to reveal the key principle of the role of H_2S. Firstly, as shown in Figs. S15 and S16 after PCM entered the substantia nigra (SN), it could co-locate significantly with NeuN (a marker representing neurons), while less co-locate with GFAP (a marker representing Astrocyte), indicated that PCM can effectively enter neurons to play a role. Then, the ROS level in SN of mouse brain was characterized, as shown in Fig. 7a and S17. Compared with the ROS level in the SN region of normal mice, the model group showed a significant increase in ROS level (2.4 times, Fig. 7b). After treatment with free small molecule H_2S donor GYY4137 and non-nanomotor based H_2S donor PTM@G, ROS levels decreased to a certain extent, while nanomotor-based H_2S donor PCM showed the most obvious decrease in ROS levels (reduced to the same level as the normal group). The decrease of ROS was conducive to reducing neuroinflammation in the SN region, while microglia activated damaged neurons by releasing inflammatory factors and other substances. Ionized calcium binding adapter molecule 1 (Iba-1) as the activation marker of microglia, was closely related to neuroinflammation. The up regulation of Iba-1 indicates the activation of microglia [48,49]. Therefore, we continued to evaluate the expression of Iba-1 in the SN region to reflect the level of inflammation. As shown in Fig. 7a and S18, compared with the normal mice, the Iba-1 positive cells in the SN region of the model mice were significantly up-regulated (increased by about 2.0 times, Fig. 7c). After treatment with different samples, the number of Iba-1 positive cells in the SN region of the mice decreased, in addition, compared to PTM, PCM can achieve more co-localization with Iba-1 (Figs. S15 and S16), this indicated that nanomotor-based H_2S donor PCM can produce H_2S in glial cells and play a role in reducing inflammation, some studies indicated that H_2S could eliminate inflammation by inducing Nrf2-Keap1 pathway to increase the transcription of anti-inflammatory genes [5] and induce microglia to return to the resting state. It was worth noting that compared with other sample groups, nanomotor-based H_2S donor PCM could more effectively eliminate neuroinflammation (reduced to the same level as the normal group), which might be due to the movement effect of nanomotor that can promote PCM to enter cells better, and then to reach the mitochondria, to play a better role. In addition to Iba-1, anti-inflammatory factors in the midbrain (where the SN was located) such as Transforming growth factor-β (TGF-β) and Interleukin-10 (IL-10) were also selected as indicators to evaluate the level of inflammation. As shown in Fig. 7d–e, the content of TGF-β and IL-10 in nanomotor-based H_2S donor PCM treatment group were significantly higher than that in the model group, western blotting analysis showed that the IL-10 levels in nanomotor-based H_2S donor PCM treatment group were much lower than that in model group (Fig. S22), verifying that nanomotor-based H_2S donor PCM could effectively promote the transcription of anti-inflammatory factors. In addition to effectively eliminating ROS and neuroinflammation, it has also been reported that H_2S could modify the Parkin protein by sulfhydration in neuron cells to increase its E3 ubiquitin ligase activity and promote the degradation of toxic proteins by proteasome [1,3,4]. Therefore, we verified the degradation of α-syn aggregates by nanomotor-based H_2S donor PCM. As shown in Fig. 7a and S19, the green fluorescence signal of α-syn aggregates in the model group was the strongest. After treatment with different forms of H_2S donors, the red fluorescence signal of α-syn aggregates decreased to a certain extent, while the nanomotor-based H_2S donor PCM group showed the least α-syn aggregates. Western blotting analysis also showed that the expression level of α-syn in the midbrain of mice treated with nanomotor-based H_2S donor PCM was comparable to that of the normal group (Fig. S22).

The above results showed that compared with free small molecule H_2S donors and passively loaded H_2S donors, nanomotor-based H_2S donor PCM had more significant functions of reducing ROS, neuroinflammation and degrading α-syn aggregates, which could ultimately promote the repair of neurons. Therefore, we also evaluated the repair of neurons, and selected tyrosine hydroxylase (TH) and neuron specific protein growth associated protein-43 (GAP-43) as indicators to represent dopamine neurons [50]. As shown in Fig. 7g, h and S19, the green fluorescence signal of TH representing dopamine neurons in the nanomotor-based H_2S donor PCM treatment group was significantly enhanced. Western blotting analysis also demonstrated a significant increase in TH expression in the midbrain of nanomotor-based H_2S donor PCM treated mice (Fig. S22), indicating that they had a positive effect on neuronal repair. At the same time, the content of GAP-43 in the SN region of the model group mice was far lower than that of the normal mice, while the level of GAP-43 in the SN region of the nanomotor-based H_2S donor PCM treated mice could be increased, indicating that

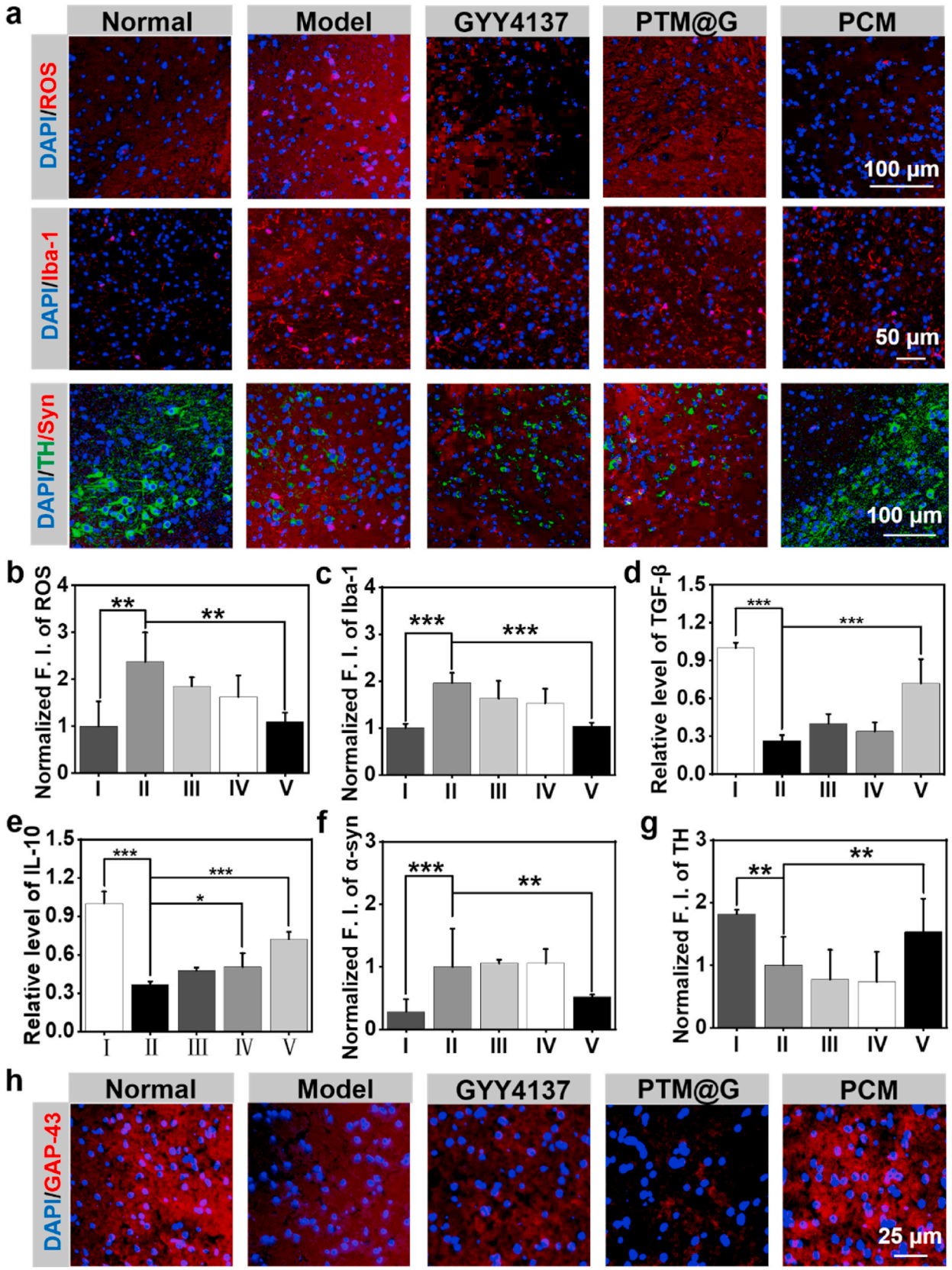

Fig. 7. Therapeutic effect *in vivo*. a) Immunofluorescence staining for ROS (red), Iba-1 (red) and α-syn aggregates (green) in the SN of mice treated by different samples; b,c) Fluorescence quantification of ROS, Iba-1 in the SN of mice treated by different samples (n = 3); Relative quantification of TGF-β (d), IL-10 (e) in the midbrain of mice treated by different samples (n = 3). f) Fluorescence quantification of α-syn aggregates in the SN of mice treated by different samples (n = 3); g) Fluorescence quantification of TH in the SN of mice treated by different samples (n = 3) and h) Immunofluorescence staining for TH (red) and GAP-43 (red) in the SN of mice treated by different samples. I: Normal; II: Model; III: GYY4137; IV: Non-nanomotor PTM@G; V: Nanomotor-based H_2S donor PCM. *$p < 0.05$, **$p < 0.01$, and ***$p < 0.001$.

nanomotor-based H_2S donor PCM had a positive effect on nerve regeneration (Fig. 7h, S20 and S21). The process of neuronal repair might be attributed to the positive effect of upregulating anti-inflammatory factors and reducing α-syn aggregates. The main organs (heart, liver, spleen, lung, kidney) of mice in different sample treatment groups were observed under the light microscope with hematoxylin/eosin (H&E) staining to evaluate the biological safety of nanomotor-based H_2S donor PCM. As shown in Fig. S23, the morphology of the main organs in each treatment group was like that in the normal group, without obvious damage, indicating that PCM had good biocompatibility. In addition, the H&E staining results in the brain showed that the number of neurons in the midbrain of model group mice was significantly reduced, and the number of cells returned to the same level as the normal group after treatment with nanomotor-based H_2S donor PCM. This indicates that nanomotor-based H_2S donor PCM can effectively rescue MPTP-induced neuronal cell damage (Figs. S24 and S25). Blood routine analysis also showed that most blood parameters of PD mice treated with PCM were similar to those of normal mice, indicating that the blood toxicity of PCM was relatively low (Table S2).

3. Conclusion

Imitating the biochemical reaction *in vivo*, we proposed a nanomotor-based H_2S donor, which had the ability to penetrate the BBB. The movement effect of the nanomotor could make it more easily entered the neuron cells selectively and reached the mitochondria through the chemotactic effect. H_2S gas signal molecules generated by the nanomotor could mediate the elimination of ROS, neuroinflammation and α-syn aggregates, thus reducing the damage of neurons and promoting the growth of nerves. Finally, animal experiments showed that this nanomotor-based H_2S donor had a good therapeutic effect on MPTP-induced PD mice.

Ethics approval and consent to participate

All the animal experiments were performed in the precondition of the animal protocol approved by the Animal Care Committee at Nanjing Normal University (Nanjing, China), and the approved number was IACUC-20200802-1.

CRediT authorship contribution statement

Zinan Zhao: Methodology, Writing – original draft, Validation, Formal analysis, Investigation, Data curation, Visualization. **Lin Chen:** Formal analysis. **Chunhao Yang:** Data curation. **Wenyan Guo:** Validation. **Yali Huang:** Investigation. **Wenjing Wang:** Data curation, Formal analysis. **Mimi Wan:** Conceptualization, Methodology, Writing – review & editing, Resources, Supervision, Project administration. **Chun Mao:** Conceptualization, Methodology, Writing – review & editing, Resources, Supervision, Project administration, Funding acquisition. **Jian Shen:** Resources, Funding acquisition.

Declaration of competing interest

The authors declare that they have no known competing financial interests or personal relationships that could have appeared to influence the work reported in this paper.

Acknowledgements

The work was supported by National Natural Science Foundation of China (No:22175096, No:22275095), Qinglan Project Foundation of Colleges and Universities of Jiangsu Province, Jiangsu Collaborative Innovation Center of Biomedical Functional Materials, Priority Academic Program Development of Jiangsu Higher Education Institution.

Appendix A. Supplementary data

Supplementary data to this article can be found online at https://doi.org/10.1016/j.bioactmat.2023.09.001.

References

[1] K.K.K. Chung, B. Thomas, X.J. Li, O. Pletnikova, J.C. Troncoso, L. Marsh, V. L. Dawson, T.M. Dawson, S-nitrosylation of parkin regulates ubiquitination and compromises parkin's protective function, Science 304 (5370) (2004) 1328–1331.
[2] T.J. Krzystek, R. Banerjee, L. Thurston, J.Q. Huang, K. Swinter, S.N. Rahman, T. L. Falzone, S. Gunawardena, Differential mitochondrial roles for α-synuclein in DRP1-dependent fission and PINK1/Parkin-mediated oxidation, Cell Death Dis. 12 (769) (2021) 796.
[3] M.S. Vandiver, B.D. Paul, R.S. Xu, S. Karuppagounder, F. Rao, A.M. Snowman, H. S. Ko, Y.I. Lee, V.L. Dawson, T.M. Dawson, N. Sen, S.H. Snyder, Sulfhydration mediates neuroprotective actions of parkin, Nat. Commun. 4 (2013) 1626.
[4] E. Chung, Y. Choi, J. Park, W. Nah, J. Park, Y. Jung, J. Lee, H. Lee, S. Park, S. Hwang, S. Kim, J. Lee, D. Min, J. Jo, S. Kang, M. Jung, P.H. Lee, H.E. Ruley, D. Jo, Intracellular delivery of parkin rescues neurons from accumulation of damaged mitochondria and pathological α-synuclein, Sci. Adv. 6 (2020), eaba1193.
[5] G.D. Yang, K.X. Zhao, Y.J. Ju, S. Mani, Q.H. Cao, S. Puukila, N. Khaper, L.Y. Wu, R. Wang, Hydrogen sulfide protects against cellular senescence via S-sulfhydration of keap1 and activation of Nrf2, Antioxidants Redox Signal. 18 (15) (2013) 1906–1919.
[6] W. Jiang, W. Zou, M. Hu, Q. Tian, F. Xiao, M. Li, P. Zhang, Y.J. Chen, J.M. Jiang, Hydrogen sulphide attenuates neuronal apoptosis of substantia nigra by re-establishing autophagic flux via promoting leptin signalling in a 6-Hydroxydopamine rat model of Parkinson's disease, Clin. Exp. Pharmacol. Physiol. 49 (1) (2022) 122–133.
[7] Y. Kimura, Y.I. Goto, H. Kimura, Hydrogen sulfide increases glutathione production and suppresses oxidative stress in mitochondria, Antioxidants Redox Signal. 12 (1) (2010) 1–13.
[8] D. Giovinazzoa, B. Bursacb, J.I. Sbodioa, S. Nallurua, T. Vignaneb, A. M. Snowmana, L.M. Albacarysa, T.W. Sedlakc, R. Torregrossad, M. Whitemand, M. R. Filipovicb, S.H. Snydera, B.D. Paul, Hydrogen sulfide is neuroprotective in Alzheimer's disease by sulfhydrating GSK3β and inhibiting Tau hyperphosphorylation, Proc. Natl. Acad. Sci. U.S.A. 118 (4) (2021), e2017225118.
[9] M. Lee, A. Sparatore, P. Del Soldato, E. McGeer, P.L. McGeer, Hydrogen sulfide-releasing NSAIDs attenuate neuroinflammation induced by microglial and astrocytic activation, Glia 58 (1) (2010) 103–113.
[10] R.A. Mohammed, S.M. Mansour, Sodium hydrogen sulfide upregulates cystathionine β-synthase and protects striatum against 3-nitropropionic acid-induced neurotoxicity in rats, J. Pharm. Pharmacol. 73 (3) (2021) 310–321.
[11] X. Cao, L. Cao, L. Ding, J.S. Bian, A new hope for a devastating disease: hydrogen sulfide in Parkinson's disease, Mol. Neurobiol. 55 (5) (2018) 3789–3799.
[12] E.R. DeLeon, G.F. Stoy, K.R. Olson, Passive loss of hydrogen sulfide in biological experiments, Anal. Biochem. 421 (1) (2012) 203–207.
[13] M.R. Sarookhani, H. Haghdoost-Yazdi, A. Sarbazi-Golezari, A. Babayan-Tazehkand, N. Rastgoo, Involvement of adenosine triphosphate-sensitive potassium channels in the neuroprotective activity of hydrogen sulfide in the 6-Hydroxydopamine-induced animal model of Parkinson's disease, Behav. Pharmacol. 29 (4) (2018) 336–343.
[14] P.K. Kamat, P. Kyles, A. Kalani, N. Tyagi, Hydrogen sulfide ameliorates homocysteine-induced Alzheimer's disease-like pathology, blood-brain barrier disruption, and synaptic disorder, Mol. Neurobiol. 53 (4) (2016) 2451–2467.
[15] Z.N. Zhao, W.Y. Guo, C.W. Xu, Q. Wang, C. Mao, M.M. Wan, Physiological functions and donor design of hydrogen sulfide and its application in central nervous system diseases, Chem. Eng. J. 452 (2023), 139089.
[16] Y.Q. Zheng, B.C. Yu, K.L. Ji, Z.X. Pan, V. Chittavong, B.H. Wang, Esterase-sensitive prodrugs with tunable release rates and direct generation of hydrogen sulfide, Angew. Chem. Int. Ed. 55 (14) (2016) 4514–4518.
[17] J.M. Kang, Z. Li, C.L. Organ, C.M. Park, C.T. Yang, A. Pacheco, D.F. Wang, D. J. Lefer, M. Xian, pH-controlled hydrogen sulfide release for myocardial ischemia-reperfusion injury, J. Am. Chem. Soc. 138 (20) (2016) 6336–6339.
[18] M.Y. Yao, Y.F. Lu, L. Shi, Y. Huang, Q. Zhang, J.L. Tan, P. Hu, J.X. Zhang, G.X. Luo, N. Zhang, A ROS-responsive, self-immolative and self-reporting hydrogen sulfide donor with multiple biological activities for the treatment of myocardial infarction, Bioact. Mater. 9 (2022) 168–182.
[19] J.S. Suk, Q.G. Xu, N. Kim, J. Hanes, L.M. Ensign, PEGylation as a strategy for improving nanoparticle-based drug and gene delivery, Adv. Drug Deliv. Rev. 99 (2016) 28–51.
[20] L. Han, C.Y. Liu, H.Z. Qi, J.H. Zhou, J. Wen, D. Wu, D. Xu, M. Qin, J. Ren, Q. X. Wang, L.X. Long, Y. Liu, I. Chen, X.B. Yuan, Y.F. Lu, C.S. Kang, Systemic delivery of monoclonal antibodies to the central nervous system for brain tumor therapy, Adv. Mater. 31 (19) (2019), 1805697.
[21] D. Wu, M. Qin, D. Xu, L. Wang, C.Y. Liu, J. Ren, G. Zhou, C. Chen, F.M. Yang, Y. Y. Li, Y. Zhao, R.Y. Huang, S. Pourtaheri, C.S. Kang, M. Kamata, I.S.Y. Chen, Z. L. He, J. Wen, W. Chen, Y.F. Lu, A bioinspired platform for effective delivery of protein therapeutics to the central nervous system, Adv. Mater. 31 (18) (2019), 1807557.
[22] T. Azuma, R. Ohmori, Y. Teramura, T. Ishizaki, M. Takai, Nano-structural comparison of 2-methacryloyloxyethyl phosphorylcholine- and ethylene glycol-

based surface modification for preventing protein and cell adhesion, Colloid. Surface. B 159 (2017) 655–661.
[23] N. Shibuya, M. Tanaka, M. Yoshida, Y. Ogasawara, T. Togawa, K. Ishii, H. Kimura, 3-Mercaptopyruvate sulfurtransferase produces hydrogen sulfide and bound sulfane sulfur in the brain, Antioxidants Redox Signal. 11 (4) (2009) 703–714.
[24] W.M. Zhao, J. Zhang, Y.J. Lu, R. Wang, The vasorelaxant effect of H_2S as a novel endogenous gaseous K_{ATP} channel opener, EMBO J. 20 (21) (2001) 6008–6016.
[25] B. Garipcan, M. Andaç, L. Uzun, A. Denizli, Methacryloylamid ocysteine functionalized poly (2-hydroxyethyl methacrylate) beads and its design as a metal-chelate affinity support for human serum albumin adsorption, React. Funct. Polym. 59 (2) (2004) 119–128.
[26] E. Özgür, H.U. Uyanık, S. Şenelc, L. Uzun, Immunoaffinity biosensor for neurofilament light chain detection and its use in Parkinson's diagnosis, Mater. Sci. Eng. B 56 (2020), 114545.
[27] Q. Wang, T. Li, J.Y. Yang, Z.N. Zhao, K.Y. Tan, S.W. Tang, M.M. Wan, C. Mao, Engineered exosomes with independent module/cascading function for therapy of Parkinson's disease by multistep targeting and multistage intervention method, Adv. Mater. 34 (27) (2022), 2201406.
[28] Z.Y. Liu, T. Li, N. Li, Y.J. Wang, L. Chen, X.T. Tang, M.M. Wan, C. Mao, GSH-induced chemotaxis nanomotors for cancer treatment by ferroptosis strategy, Sci. China Chem. 65 (5) (2022) 989–1002.
[29] H.D. Shen, Q. Liu, D.J. Liu, S.S. Yu, X. Wang, M.B. Yang, Fabrication of doxorubicin conjugated methoxy poly(ethylene glycol)-block-poly(ε-caprolactone) nanoparticles and study on their in vitro antitumor activities, J. Biomater. Sci. Polym. Ed. 32 (13) (2021) 1703–1717.
[30] Y. Zhao, H. Wang, M. Xian, Cysteine-activated hydrogen sulfide (H_2S) donors, J. Am. Chem. Soc. 133 (1) (2011) 15–17.
[31] Y. Zhao, S.S. Bhushan, C.T. Yang, H. Otsuka, J.D. Stein, A. Pacheco, B. Peng, N. O. Devarie-Baez, H.C. Aguilar, D.J. Lefer, M. Xian, Controllable hydrogen sulfide donors and their activity against myocardial ischemia-reperfusion injury, ACS Chem. Biol. 8 (6) (2013) 1283–1290.
[32] C.R. Powell, J.C. Foster, B. Okyere, M.H. Theus, J.B. Matson, Therapeutic delivery of H_2S via COS: small molecule and polymeric donors with benign byproducts, J. Am. Chem. Soc. 138 (41) (2016) 13477–13480.
[33] P.Y.H. Chen, R.H. Zhao, C. Tang, C. Zhang, W.Y. Xu, L.Y. Wu, Y.Q. Wang, D.J. Ye, Y. Liang, Design and development of a bioorthogonal, visualizable and mitochondria-targeted hydrogen sulfide (H_2S) delivery system, Angew. Chem. Int. Ed. 61 (6) (2022), e202112734.
[34] Y.Y. Yuan, C.Q. Mao, X.J. Du, J.Z. Du, F. Wang, J. Wang, Surface charge switchable nanoparticles based on zwitterionic polymer for enhanced drug delivery to tumor, Adv. Mater. 24 (40) (2012) 5476–5480.
[35] S. Ashraf, J. Park, M.A. Bichelberger, K. Kantner, R. Hartmann, P. Maffre, A. H. Said, N. Feliu, J. Lee, D. Lee, G.U. Nienhaus, S. Kim, W.J. Parak, Zwitterionic surface coating of quantum dots reduces protein adsorption and cellular uptake, Nanoscale 8 (41) (2016) 17794–17800.
[36] W.H. Ji, Y. Li, H. Peng, R.C. Zhao, J. Shen, Y.Y. Wu, J.Z. Wang, Q.L. Hao, Z.G. Lu, J. Yang, X. Zhang, Self-catalytic small interfering RNA nanocarriers for synergistic treatment of neurodegenerative diseases, Adv. Mater. 34 (1) (2022), 2105711.
[37] Z.X. Fan, T. Ren, Y.J. Wang, H. Jin, D. Shi, X.F. Tan, D.T. Ge, Z.Q. Hou, X. Jin, L. C. Yang, Aβ-responsive metformin-based supramolecular synergistic nanodrugs for Alzheimer's disease via enhancing microglial Aβ clearance, Biomaterials 283 (2022), 121452.
[38] Y. Liu, P. Hu, Z.H. Zheng, D. Zhong, W.C. Xie, Z.B. Tang, B.X. Pan, J. Luo, W. H. Zhang, X.L. Wang, Photoresponsive vaccine-like CAR-M system with high-efficiency central immune regulation for inflammation-related depression, Adv. Mater. 34 (11) (2022), 2108525.
[39] M.M. Wan, Q. Wang, X.Y. Li, B. Xu, D. Fang, T. Li, Y.Q. Yu, L.Y. Fang, Y. Wang, M. Wang, F.H. Wang, C. Mao, J. Shen, J. Wei, Systematic research and evaluation models of nanomotors for cancer combined therapy, Angew. Chem. Int. Ed. 59 (34) (2020) 14458–14465.
[40] J. E Parada, A. Egea, L. Romero, D. Barrio, A.G. García, M.G. López, Poststress treatment with PNU282987 can rescue SH-SY5Y cells undergoing apoptosis via α7 nicotinic receptors linked to a Jak2/Akt/HO-1 signaling pathway, Free Radical Biol. Med. 49 (11) (2010) 1815–1821.
[41] H.Y. Yue, E. Bieberich, J.H. Xu, Promotion of endocytosis efficiency through an ATP-independent mechanism at rat calyx of held terminals, J. Physiol. 595 (15) (2017) 5265–5284.
[42] F.Z. Mou, Q. Xie, J.F. Liu, S.P. Che, L. Bahmane, M. You, J.G. Guan, ZnO-based micromotors fueled by CO_2: the first example of self-reorientation-induced biomimetic chemotaxis, Natl. Sci. Rev. 8 (11) (2021) nwab066.
[43] K. Xiong, L.L. Xu, J.W. Lin, F.Z. Mou, J.G. Guan, Mg-based micromotors with motion responsive to dual stimuli, Research 2020 (2020), 6213981.
[44] L. Li, M. Whiteman, Y.Y. Guan, K.L. Neo, Y. Cheng, S.W. Lee, Y.J. Zhao, R. Baskar, C.H. Tan, P.K. Moore, Characterization of a novel, water-soluble hydrogen sulfide-releasing molecule (GYY4137), Circulation 117 (18) (2018) 2351–2360.
[45] M. Sahin, G. Oncu, M.A. Yilmaz, D. Ozkan, H. Saybasili, Transformation of SH-SY5Y cell line into neuron-like cells: Investigation of electrophysiological and biomechanical changes, Neurosci. Lett. 745 (2021), 135628.
[46] S.P. Presgraves, T. Ahmed, S. Borwege, J.N. Joyce, Terminally differentiated SH-SY5Y cells provide a model system for studying neuroprotective effects of dopamine agonists, Neurotex. Res. 5 (8) (2004) 579.
[47] L.Y. Liu, Y. Li, R.Y. Liu, Q. Shen, Y.H. Li, Z.Y. Shi, J. Shen, W.H. Jia, X. Zhang, Switchable nanoparticle for programmed gene-chem delivery with enhanced neuronal recovery and CT imaging for neurodegenerative disease treatment, Mater. Horiz. 6 (9) (2019) 1923–1929.
[48] H.H. Liu, Y.B. Han, T.T. Wang, H. Zhang, Q. Xu, J.X. Yuan, Z. Li, Targeting microglia for therapy of Parkinson's disease by using biomimetic ultrasmall nanoparticles, J. Am. Chem. Soc. 142 (52) (2020), 21730.
[49] A.A. Hamdan, H.G. Bounihi, V. Lenoir, M. Andriamihaja, F. Blachier, F. Bouillaud, Chapter twelv -oxidation of H_2S in mammalian cells and mitochondria, Methods Enzymol. 554 (2015) 201–228.
[50] Y.Q. Jiang, P.F. Fu, Y.Y. Liu, C.C. Wang, P.R. Zhao, X. Chu, X.W. Jiang, W. Yang, Y. L. Wu, Y. Wang, G.H. Xu, J. Hu, W.B. Bu, Near-infrared light-triggered NO release for spinal cord injury repair, Sci. Adv. 6 (39) (2020) eabc3513.